Online Voltage Stability Assessment for Load Areas Based on the Holomorphic Embedding Method

Liu, Chengxi ; Wang, Bin; Hu, Fengkai; Sun, Kai; Bak, Claus Leth

Published in:
I E E E Transactions on Power Systems

DOI (link to publication from Publisher):
10.1109/TPWRS.2017.2771384

Publication date:
2018

Document Version
Accepted author manuscript, peer reviewed version

This article has been accepted for publication in a future issue of this journal, but has not been fully edited. Content may change prior to final publication. Citation information: DOI 10.1109/TPWRS.2017.2771384, IEEE Transactions on Power Systems

Online Voltage Stability Assessment for Load Areas Based on the Holomorphic Embedding Method

Chengxi Liu *Member, IEEE*, Bin Wang, *Student Member*, Fengkai Hu, *Student Member, IEEE*, Kai Sun, *Senior Member IEEE*, and Claus Leth Bak, *Senior Member IEEE*

***Abstract*—This paper proposes an online steady-state voltage stability assessment scheme to evaluate the proximity to voltage collapse at each bus of a load area. Using a non-iterative holomorphic embedding method (HEM) with a proposed physical germ solution, an accurate loading limit at each load bus can be calculated based on online state estimation on the entire load area and a measurement-based equivalent for the external system. The HEM employs a power series to calculate an accurate P-V curve at each load bus and accordingly evaluates the voltage stability margin considering load variations in the next period. An adaptive two-stage Padé approximant method is proposed to improve the convergence of the power series for accurate determination of the nose point on the P-V curve with moderate computational burden. The proposed method is first illustrated in detail on a 4-bus test system and then demonstrated on a load area of the Northeast Power Coordinating Council 48-geneartor, 140-bus power system.**

***Index Terms*—Continuation power flow, holomorphic embedding method, Padé approximant, voltage stability assessment, voltage stability margin.**

I. Introduction

THE increase of electrical energy demand and the obstacle of concomitant infrastructure upgrading have driven electrical power systems operated closer to their stability limits. At present, electricity utilities are more concerned about the issues of voltage stability. A reliable, accurate, fast, online voltage stability assessment (VSA) is critical in the operational environment for the utilities to not only identify areas vulnerable to voltage instability, especially under stressed system conditions, but also provide system operators with first-hand advices on control actions.

Based on the online state estimation of operating conditions and the dependable power system models, many model-based VSA methods are utilized to estimate the voltage stability margin (VSM) of a power system, such as the modal analysis method [1]-[3], singular value decomposition method [4], [5], voltage sensitivity method [6], [7], bifurcation theory-based method [8], [9] and continuation power flow (CPF) [10]. In CPF, the system load is increased in a certain way until the maximum loading point is reached. By iteratively performing a prediction-correction scheme, the CPF can preserve the nonlinearity of power flow equations (PFEs) and overcome the singularity problem. However, its computational burden due to iterations is a major concern for online applications.

At present, many utilities have also deployed synchronized phasor measurement units (PMUs) on transmission systems to provide the real-time voltage stability monitoring. Many measurement-based VSA approaches approximate the external system by estimating parameters of a Thevenin equivalent circuit. They rely on real-time synchronized phasor data from PMUs placed on the boundary of a load area [11]-[17]. Because the full observability on all buses in the load area in real time is often unavailable, a widely adopted approach is to offline reduce the load area to either an equivalent load bus or an equivalent simplified network and to online identify the parameters including those for the external system using PMU data. These measurement-based methods can assess voltage stability of a load area on its boundary but lack the monitoring of each bus in the area and depend on the accurate identification of equivalent parameters, which is often difficult in the case of fast load variations.

This paper proposes an online hybrid VSA scheme to predict voltage instability of a load area by power flow calculations using a derivative holomorphic embedding method (HEM). An accurate loading limit at each load bus in the load area can be calculated based on online state estimation on the entire load area and a measurement-based equivalent for the external system. A power series in an embedded complex variable on the load level is derived by the HEM. A *physical germ* solution is proposed to ensure that the embedded value of the power series is always equal to the overall loading level of the load area. Therefore, fed by on-line data on active and reactive powers at each load bus, the P-V (Power-Voltage) curve for every bus can be accurately calculated by performing only one-time HEM calculation compared to many iterative computations with CPF. Besides, the adoption of adaptive Padé approximant (PA) for the power series given by the HEM can guarantee its convergence near voltage collapse, so as to accurately locate the voltage collapse point. Superior to other power-flow calculation methods, the

This work was supported in part by CURENT Engineering Research Center and NSF grant ECCS-1610025.

C. Liu, B. Wang and K. Sun are with the Department of EECS, University of Tennessee, Knoxville, TN, USA (email: cliu48@utk.edu, kaisun@utk.edu, bwang@utk.edu).

F. Hu is with Siemens Industry, Inc., Minneapolis, MN, USA (email: fengkai.hu@siemens.com).

C. L. Bak is with the Department of Energy, Aalborg University, Aalborg, Denmark (email: clb@et.aau.dk).

This article has been accepted for publication in a future issue of this journal, but has not been fully edited. Content may change prior to final publication. Citation information: DOI 10.1109/TPWRS.2017.2771384, IEEE Transactions on Power Systems

HEM analytically gives the P-V curve connecting the current operating point to the voltage collapse point for an anticipated scenario of load increase, such that the VSM is directly obtained. Compared with other VSA methods, the proposed online HEM-based VSA approach can estimate the VSM at each bus of a load area and predict voltage instability with better time performance.

As a promising non-iterative method for solving PFEs of large power systems, the HEM was first proposed by A. Trias [18]-[20]. Its basic idea is to design a holomorphic function and adopt its analytic continuation in the complex plane in order to find a power flow solution in a form of power series. The coefficients of power series are calculated in a recursive manner, whose numerical divergence means non-existence of the solution. The HEM was first demonstrated on systems having only PQ buses and a slack bus [18], and then on systems having PV buses as well [21]-[28]. To enhance the convergence of the derived power series, references [18]-[28] suggest using PA, continued fractions or a multi-stage strategy. Reported HEM applications include analysis of saddle-node bifurcation [29], power flows of hybrid AC/DC systems [31], finding unstable equilibrium points [32], [33], network reduction [34], analysis of limit-induced bifurcation [35].

Although the superiority of the HEM can be seen in literatures, its practical implementation may encounter a precision issue especially for heavily loaded systems [33], [36]. Moreover, these previous HEMs are devoted to find the solution of one specific load condition, so their embedded variables unnecessarily have a physical meaning, e.g. the actual loading level. In [29], the HEM is applied to estimate the saddle-node bifurcation point of static power flow conditions, in which the loads and total generation are scaled at the same rate. Compared with [29], a hybrid VSA approach is applied and demonstrated on a realistic power network, where loads and generation can be scaled independently.

In [30], the P-V curve can be drawn by a derivative HEM using the error embedding algorithm. However, it is a multi-stage method, so the analytical solutions of the P-V curve can not be directly obtained from one-time computation. Furthermore, supplemented with load trending prediction, this approach can predict the trend of voltage for early warning of voltage instability for system operators. Fast performance of the HEM gives the operators enough time to respond to foreseen instability and take necessary remedial actions.

The rest of this paper is organized as follows. Section II introduces the conventional HEM algorithm. Section III proposes a derivative embedding method starting from a physical germ solution on P-V curves. Section IV proposes an adaptive PA method to increase the accuracy. Section V introduces the novel VSA approach in detail, including the parameter identification of the external grid, online VSA scheme, analysis of computation burden, etc. Section VI uses a 4-bus test system to demonstrate the advantages of this new method. Section VII tests the scheme on a load area of the Northeast Power Coordinating Council (NPCC) power system. Finally, conclusions are drawn in Section VII.

II. Conventional Holomorphic Embedding Load Flow Method

Consider a complex-valued function $x(s)$ of complex variable $s = p+iq$, with real part p and imaginary part q. If the embedded complex-valued function $x(p+iq)$ satisfies Cauchy-Riemann equation (1), $x(s)$ is complex-differentiable and thus holomorphic in a neighborhood of the complex s-plane [37].

$$i\frac{\partial x}{\partial p} = \frac{\partial x}{\partial q} \tag{1}$$

Under this circumstance, $x(s)$ can be represented in the form of power series (2) in s within its convergence region $\boldsymbol{C}$.

$$x(s) = \sum_{n=0}^{\infty} x[n]s^n, s \subset \boldsymbol{C} \tag{2}$$

In order to solve a nonlinear equation $g(x) = 0$, substitute (2) for x to generate a composite function of embedded variable s:

$$g(x) = g[x(s)] = 0. \tag{3}$$

The idea of using the HEM to solve power flows is to embed a complex variable s into the nonlinear PFEs such that in the complex s-plane, an analytical solution is originated from a common germ solution and expanded to the objective final solution. Therefore, the power-flow problem becomes how to design an $x(s)$ satisfying the following four criteria:

1) A common *germ* solution at $s = 0$ can be found for the equation $g[x(s)] = 0$. For power flow calculation, the germ solution is conventionally designated as the solution under a no-load, no-generation condition.
2) Ensuring that $g[x(s)] = 0$ also holds at $s = 1$ and the power series (2) can be mathematically induced within a defined number of order N, through expanding and equating the coefficients of the same order of s^n in $g[x(s)] = 0$. Thus, the final solution of x is easily obtained by letting $s = 1$ in (2).
3) The s-embedded complex function $g[x(s)]$ is analytically continuous (holomorphic) along the path from the germ solution at $s = 0$ to the final solution at $s = 1$.
4) On the path of s before bifurcation occurs, there is no exceptional point (also called branch point) where multiple solutions of $g[x(s)] = 0$ coalesce with each other. Exceptional points only coincide at the bifurcation point.

Consider an N-bus system composed of PQ buses, PV buses and slack buses, which are denoted as sets of $\boldsymbol{\mathcal{P}}$, $\boldsymbol{\mathcal{V}}$ and $\boldsymbol{\mathcal{S}}$ respectively. The original PFEs for PQ buses, PV buses and slack buses are expressed in the following (4)-(6) respectively,

$$\sum_{k=1}^{N} Y_{ik}V_k = \frac{(P_i + jQ_i)^*}{V_i^*}, \forall i \in \boldsymbol{\mathcal{P}} \tag{4}$$

$$\begin{cases} P_i = \mathrm{Re}\left(V_i \sum_{k=1}^{N} Y_{ik}^* V_k^*\right) \\ |V|_i = \left|V_i^{sp}\right| \end{cases}, \forall i \in \boldsymbol{\mathcal{V}} \tag{5}$$

$$V_i = V_i^{SL}, \forall i \in \boldsymbol{\mathcal{S}} \tag{6}$$

where P_i, Q_i, $|V_i|$ and θ_i are the active power injection, reactive power injection, voltage magnitude and phase angle at bus i. V_k is the voltage phasor of bus k adjacent to bus i. Y_{ik} is the admittance between bus i and bus k.

This article has been accepted for publication in a future issue of this journal, but has not been fully edited. Content may change prior to final publication. Citation information: DOI 10.1109/TPWRS.2017.2771384, IEEE Transactions on Power Systems

By the HEM formulation, the voltage of each bus and the reactive power of each PV bus are both represented as power series functions of an embedded complex variable s, denoted by $V(s)$ and $Q(s)$ respectively. Then, the s-embedded equations of PQ buses, PV buses and SL buses in (4)-(6) can be expressed as (7)-(9) respectively. Note that, in order to maintain the holomorphy of $V(s)$, its conjugate V^* is defined as a separate function $V^*(s^*)$, not $V^*(s)$. See [23] for details on conventional HEM-based load flow calculation.

$$\sum_{k=1}^{N} Y_{ik,trans} V_k(s) = \frac{sS_i^*}{V_i^*(s^*)} - sY_{i,shunt} V_i(s), \forall i \in \boldsymbol{\mathcal{P}} \tag{7}$$

$$\begin{cases} \sum_{k=1}^{N} Y_{ik,trans} V_k(s) = \dfrac{sP_i - jQ_i(s)}{V_i^*(s^*)} - sY_{i,shunt} V_i(s) \\ V_i(s) V_i^*(s^*) = 1 + \left(\left| V_i^{sp} \right|^2 - 1 \right) s \end{cases}, \forall i \in \boldsymbol{\mathcal{V}} \tag{8}$$

$$V_i(s) = 1 + (V_i^{SL} - 1)s, \forall i \in \boldsymbol{\mathcal{S}} \tag{9}$$

III. New HEM with Physical Germ Solution

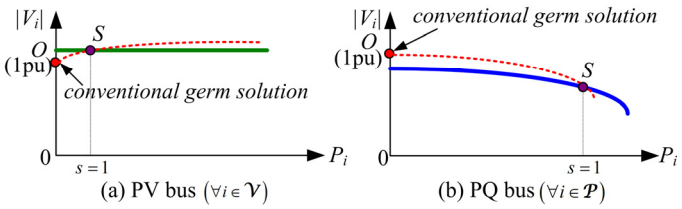

Fig. 1. The procedure of the conventional HEM.

In Eq. (7) and (8), the conventional method decomposes the admittance matrix Y_{ik} into series part $Y_{ik,trans}$ and shunt part $Y_{i,shunt}$ to ensure that the common germ solution has the voltage equal to $1\angle 0^\circ$ under the no-load, no-generation and no-shunt condition at every bus in the network, i.e. Point O in Fig. 1. Therefore, the power series expression created by the HEM (as indicated by the red dotted line) intersect the true P-V curve only at s = 1, i.e. Point S in Fig. 1(a)-(b) for the PV bus and PQ bus respectively. However, the embedded s does not mean a physical power flow solution at its other values, because $Y_{i,shunt}$ is also scaled by s in (7) and (8).

As illustrated in Fig. 2, different from the germ solution for the conventional HEM, a physical germ solution is proposed in this paper with the no-load no-generation assumption only for PQ buses while non-zero active power is specified and reactive power is injected into PV buses to adjust their voltage magnitudes specifically to $|V_i^{sp}|$, i.e. Point B in Fig. 2.

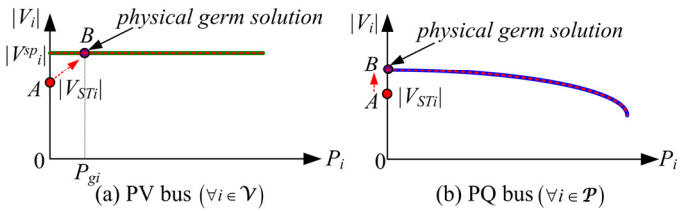

Fig. 2. The procedure of finding the physical germ solution.

Therefore, to find the physical germ, the s-embedded equations of PQ buses, PV buses and SL buses in (4)-(6) are expressed as in (10)-(12) respectively, where notations with subscript gi indicates the physical germ solution of bus i.

$$\sum_{k=1}^{N} Y_{ik} V_k(s) = 0, \forall i \in \boldsymbol{\mathcal{P}} \tag{10}$$

$$\begin{cases} \sum_{k=1}^{N} Y_{ik} V_k(s) = \dfrac{sP_{gi} - jQ_{gi}(s)}{V_{gi}^*(s^*)} \\ V_{gi}(s) V_{gi}^*(s^*) = \left| V_{STi} \right|^2 + \left(\left| V_{gi}^{sp} \right|^2 - \left| V_{STi} \right|^2 \right) s \end{cases}, \forall i \in \boldsymbol{\mathcal{V}} \tag{11}$$

$$V_{gi}(s) = V_{gi}^{SL}, \forall i \in \boldsymbol{\mathcal{S}} \tag{12}$$

The procedure of finding this physical germ solution consists of two steps. The first step is to find the starting voltage under which the slack bus propagates its voltage to every bus of the network, while all PV and PQ buses have zero injection to the grid, i.e. Point A in Fig. 2(a) and Fig. 2(b) for PV bus and PQ bus, respectively. V_{STi} in (11) represents the starting voltage of bus i, which is calculated by (13)-(14).

$$\sum_{k=1}^{N} Y_{ik} V_{STk} = V_i^{SL}, \forall i \in \boldsymbol{\mathcal{S}} \tag{13}$$

$$\sum_{k=1}^{N} Y_{ik} V_{STk} = 0, \forall i \in \boldsymbol{\mathcal{P}} \cup \boldsymbol{\mathcal{V}} \tag{14}$$

Then the second step is to gradually adjust the reactive powers of PV buses to control their voltage magnitudes from the starting voltage $|V_{STi}|$ to the specified voltage $|V^{sp}{}_i|$ by recursively embedding a series of reactive power equal to $Q_{gi}(s)$. Meanwhile, the active power of each PV bus is fixed at the base value of the original condition P_{gi}, i.e. Point B in Fig. 2(a) and Fig. 2(b) for PV bus and PQ bus respectively.

Define the voltage of the physical germ solution for bus i as $V_{gi}(s)$, which is expanded to a power series in s.

$$V_{gi}(s) = V_{STi} + V_{gi}[1]s + V_{gi}[2]s^2 + \cdots \tag{15}$$

Then define another power series $W_{gi}(s)$ as its inverse:

$$W_{gi}(s) = \frac{1}{V_{gi}(s)} = W_{gi}[0] + W_{gi}[1]s + W_{gi}[2]s^2 + \cdots \tag{16}$$

Since starting voltage V_{STi} is calculated by (13)-(14), $W_{gi}[n]$, i.e. the coefficient of term n, can be calculated by convolution of coefficients of terms 1 to n-1 of $V_{gi}(s)$ and $W_{gi}(s)$ by

$$W_{gi}[0] = 1/V_{STi} \tag{17}$$

$$W_{gi}[n] V_{STi} + W_{gi}[0] V_{gi}[n] = -\sum_{m=1}^{n-1} W_{gi}[m] V_{gi}[n-m], \quad n \geq 1 \tag{18}$$

Substitute $W_{gi}(s)$ to embedded PFEs (10)-(11) and expand them as (19) and (20) for PQ and PV buses, respectively.

$$\sum_{k=1}^{N} Y_{ik} \left(V_{STk} + V_{gk}[1]s + V_{gk}[2]s^2 + \cdots \right) = 0, \forall i \in \boldsymbol{\mathcal{P}} \tag{19}$$

$$\begin{cases} \sum_{k=1}^{N} Y_{ik} \left(V_{STk} + V_{gk}[1]s + V_{gk}[2]s^2 + \cdots \right) \\ = \left[sP_{gi} - j\left(Q_{gi}[1]s + Q_{gi}[2]s^2 + \cdots \right) \right] \left(W_{gi}^*[0] + W_{gi}^*[1]s + \cdots \right) \\ \left(V_{STi} + V_{gi}[1]s + \cdots \right) \left(V_{STi}^* + V_{gi}^*[1]s + \cdots \right) \\ = \left| V_{STi} \right|^2 + \left(\left| V_{gi}^{sp} \right|^2 - \left| V_{STi} \right|^2 \right) s \end{cases}, \forall i \in \boldsymbol{\mathcal{V}} \tag{20}$$

Equating the coefficients of s, s^2,… up to s^n on both sides of (19) and (20), $V_{gi}[n]$ and $Q_{gi}[n]$ are obtained by the terms 0 to n-1 of $W_{gi}(s)$ and $Q_{gi}(s)$ from (21) and (22).

$$\sum_{k=1}^{N} Y_{ik} V_{gk}[n] = 0, \forall i \in \boldsymbol{\mathcal{P}} \tag{21}$$

This article has been accepted for publication in a future issue of this journal, but has not been fully edited. Content may change prior to final publication. Citation information: DOI 10.1109/TPWRS.2017.2771384, IEEE Transactions on Power Systems

$$\begin{cases} \sum_{k=1}^{N} Y_{ik}V_{gk}[n] = P_i W_{gi}^*[n-1] - jQ_{gi}[n]W_{gi}^*[0] - j\left(\sum_{m=1}^{n-1} Q_{gi}[m]W_{gi}^*[n-m]\right), \forall i \in \boldsymbol{\mathcal{V}} \\ V_{gi}[n]V_{gi}^*[0] + V_{gi}[n]V_{gi}^*[0] = \varepsilon_i[n-1] \end{cases} \quad (22)$$

$\varepsilon_i[n\text{-}1]$ defined by (23) can quickly converge with a few terms since it contains the high order terms of $V_{gi}[n]s^n$.

$$\varepsilon_i[n-1] = \delta_{n1} \cdot \frac{1}{2}\left(\left|V_{gi}^{sp}\right|^2 - \left|V_{STi}\right|^2\right) - \frac{1}{2}\left(\sum_{m=1}^{n-1} V_{gi}[m]V_{gi}^*[n-m]\right) \quad (23)$$

δ_{nj} in (23) is the Kronecker delta function:

$$\delta_{nj} = \begin{cases} 1 & \text{if } n = j \\ 0 & \text{otherwise} \end{cases} \quad (24)$$

In (22), $V_{gi}[n]$ and $W_{gi}[n]$ are unknown complex numbers, and $Q_{gi}[n]$ is an unknown real number. Move all unknowns of the nth order coefficients to the left hand side and break the PFEs into real and imaginary parts. Then, a matrix equation is created containing all $V_{gi}[n]$, $W_{gi}[n]$ and $Q_{gi}[n]$. There are 5 real unknowns in total for each PV bus, as $V_{gi}[n]$ and $W_{gi}[n]$ are complex values and $Q_{gi}[n]$ is a real number. Assume that there are l slack buses, m PQ buses and p PV buses in the N-bus network. Then, the dimension of the matrix equation equals to $2l+2m+5p$. The matrix equation to find the physical germ solution of a demonstrative 3-bus system is introduced in detail in APPENDIX-A.

After obtaining the physical germ solution, the final process of the proposed HEM is similar to the conventional HEM. Table I shows the embedding method of HEM with the proposed physical germ solution for PQ, PV and SL buses, respectively, where s represents the loading level only for PQ buses. The difference mainly lies on the right hand side of PQ bus equation in Table I, that s is multiplied by the complex load of the PQ bus. Note that, different from the conventional HEM during the process of embedding, the active powers of PV buses are not multiplied by s, indicating invariant generation outputs under load increase. However, if frequency regulation is considered with PV buses, which typically models generator buses, an additional term with generation regulation factor α_i can be attached as shown in (25) to represent the effect of frequency regulation. Here $\alpha_i P_i$ represents the increase rate of active power of generator i with respect to the overall load variation.

$$\sum_{k=1}^{N} Y_{ik}V_k(s) = \frac{\left(P_{gi} - jQ_{gi}\right) + s\left(\alpha_i P_i\right) - jQ_i(s)}{V_i^*(s^*)}, \forall i \in \boldsymbol{\mathcal{V}} \quad (25)$$

TABLE I.
SOLUTIONS OF PFES FOR DIFFERENT BUS TYPES WITH THE PROPOSED HEM

Type	Physical germ solution (s = 0)	Final solution (s ≠ 0)
PQ	$\sum_{k=1}^{N} Y_{ik}V_k(s) = 0$	$\sum_{k=1}^{N} Y_{ik}V_k(s) = \frac{s(P_i - jQ_i)}{V_i^*(s^*)}$
PV	$\sum_{k=1}^{N} Y_{ik}V_k(s) = \frac{P_{gi} - jQ_{gi}}{V_{gi}^*}$ $V_i(s)V_i^*(s^*) = \left\|V_{gi}\right\|^2$	$\sum_{k=1}^{N} Y_{ik}V_k(s) = \frac{(P_{gi} - jQ_{gi}) - jQ_i(s)}{V_i^*(s^*)}$ $V_i(s)V_i^*(s^*) = \left\|V_{gi}\right\|^2 + \left(\left\|V_i^{sp}\right\|^2 - \left\|V_{gi}\right\|^2\right)s$
SL	$V_i(s) = V_i^{SL}$	$V_i(s) = V_i^{SL}$

IV. ADAPTIVE TWO-STAGE PADE APPROXIMANTS

As mentioned in the previous section, voltage can be expressed in the form of power series (26) by the HEM. However, the precision issue could have a non-ignorable impact on the performance of HEM, especially when the loading level s extends to the heavily stressed conditions [33], [36]. The reason of this problem lies in the limited convergence region of a truncated power series with limited arithmetic precision. In addition, the double-precision calculation with about 16-digits practically becomes exhausted to decrease the errors of PFEs to 1×10^{-13} or lower. An alternative solution is to increase the arithmetic precision to much more digits, i.e. 2000 digits in [36], but the convergence region still cannot reach the actual stability boundary.

From Stahl's Pade convergence theory in [38] and [39], the diagonal or close to diagonal PA converge to the original function in the maximum domain if the original function is holomorphic. In other words, PA have the best convergence performance with equal or nearly equal orders between the numerator and denominator, i.e. $|L\text{-}M| \le 1$ in (27). Different from the conventional HEM using PA to determine the convergence of PFEs [17]-[20], an adaptive two-stage algorithm is proposed here to find the optimal order of PA for each voltage. Viskovatov's method is adopted here to find the coefficients of PA [40]. This is carried out with the double precision arithmetic computation after the HEM is performed.

$$V_i(s) = \sum_{n=0}^{N} V_i[n]s^n \quad (26)$$

$$V_i(s) = \sum_{l=0}^{L} a_l s^l \Big/ \sum_{m=0}^{M} b_m s^m = \frac{a_0 + a_1 s + a_2 s^2 + \cdots + a_L s^L}{b_0 + b_1 s + b_2 s^2 + \cdots + a_M s^M} \quad (27)$$

As shown by the flowchart in Fig. 3, the adaptive PA method consists of two stages, i.e. finding a coarse collapse point at *sc'* and then identifying a precise collapse point at *sc*. The first stage is to plug values of s into the power series about PQ buses created by the HEM to find the maximum convergence region at $s = s_m$, shown by point A in Fig. 4. Then the full order PA, i.e. $[L/M]$ for the power series can improve the convergence region from $s = s_m$ to the coarse collapse point $s = sc'$, where the maximum $\varepsilon(s)$ of all PQ buses can be less than a preset threshold ε_{th}, shown by point B in Fig. 4. This process is defined by equation (28).

$$sc' = \max s, \text{ s.t.}$$
$$\varepsilon(s) = \max_i \left| \sum_{k=1}^{N} Y_{ik}V_k(s) - \frac{sS_i^*}{V_i^*(s^*)} \right|_{i \ne k} < \varepsilon_{th}, \forall i \in \boldsymbol{\mathcal{P}} \quad (28)$$

The second stage is to find the optimal order of PA for individual bus i to achieve the minimum error of PBEs at $s = sc'$ (27). The optimal order for individual bus i is recorded as L_i and M_i, so the Pade expression of voltage is obtained by truncating $[L_i/M_i]$ orders in (27) while still satisfying $|L_i\text{-}M_i| \le 1$. The collapse point of bus i is the nearest pole of the truncated PA, i.e. sc_i. Finally, the final collapse point predicted at time t, i.e. sc_t in (29), is found by selecting the minimum sc_i of all buses, shown by point C in Fig. 4.

$$sc_t = \min_i sc_i = \min_i \left(\min_{M_i \& L_i} \varepsilon(sc') \right), \forall i \in \boldsymbol{\mathcal{P}} \quad (29)$$

This article has been accepted for publication in a future issue of this journal, but has not been fully edited. Content may change prior to final publication. Citation information: DOI 10.1109/TPWRS.2017.2771384, IEEE Transactions on Power Systems

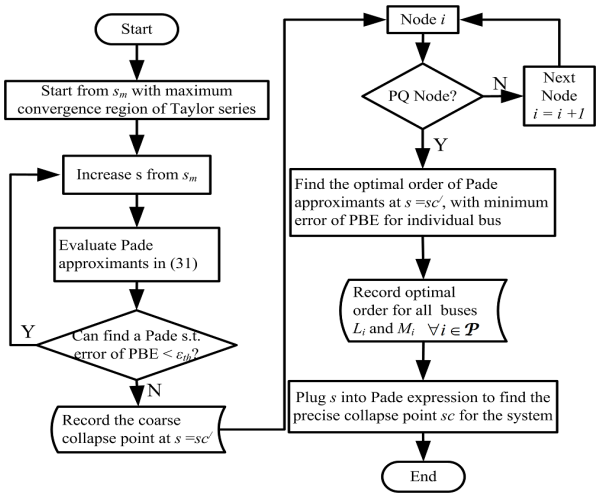

Fig. 3. Flowchart of adaptive two-stage PA to find the collapse point of the power system.

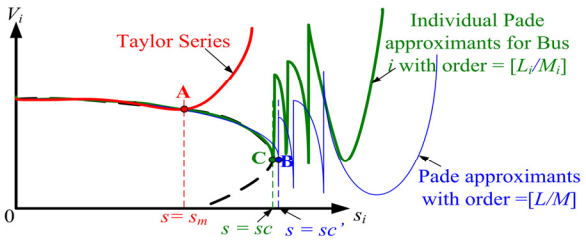

Fig. 4. Illustration of adaptive two-stage PA.

This adaptive two-stage method finds a good tradeoff between the error tolerance in the solution and the condition number of the Pade matrix. When evaluating a diagonal $[L/M]$ Pade, coefficients of terms up to s^{L+M} are required for the power series. The condition number of the Pade matrix increases as the degree of the diagonal PA increases. Due to the adopted double-precision arithmetic and the round-off errors in the calculation process, evaluating the highest degree of PA usually means adding inaccurate numbers very close to zero to the numerators and denominators of (27), which leads to an inaccurate estimation of collapse point [23]. Therefore, adaptively adjusting to an appropriate degree of PA for each load bus can increase the accuracy.

V. Online Voltage Stability Assessment

Online VSA scheme by the HEM is proposed to predict voltage instability of a load area. The parameters of equivalent circuit are identified to represent the external grid. Then, an accurate loading limit at each load bus in the load area can be calculated based on the state estimation on the entire load area.

A. Identification of External System Parameters

Suppose a load area fed by an external system through multiple tie lines. These tie lines may have different power transfer limits in terms of voltage stability. As shown in red in Fig. 5, an N+1 buses equivalent system representing the external grid is proposed in [14]. The external grid is regarded as a single voltage source E connected to N boundary buses of the load area respectively by N branches with impedances z_{E1} to z_{EN}. Therefore, the coupling relationship among tie lines and boundary buses are retained, so the HEM-based online VSA scheme can be performed directly on the reduced system as in Fig. 5, while retaining all load buses in the load area.

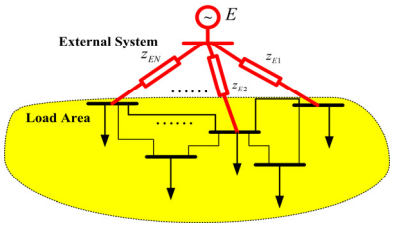

Fig. 5. Reduction of the external system to an N+1 equivalent circuit.

The Sequential Quadratic Programming (SQP) method in [41] is applied to identify the parameters of the equivalent circuit, i.e. E and z_{E1} to z_{EN}, using synchronized data of complex power S_i and voltage phasor V_i measured at the boundary buses. Assume that a time window of K measurement points is obtained by PMUs. $V_i(k) = |V_i(k)| \angle \theta_i(k)$ and $S_i(k) = P_i(k) + jQ_i(k)$ are defined respectively as the received complex power and voltage phasor at boundary bus i at time point k (k=1~K). Therefore, the parameters of the external system can be obtained by solving the following optimization problem,

$$\min J^{ex} = \sum_{k=1}^{K}\sum_{i=1}^{N}\frac{\omega_e}{N}\left[e_i^{ex}(k)\right]^2 + \sum_{i=1}^{N}\omega_z\left(\frac{r_{Ei}}{r_{EP}}-1\right)^2 + \sum_{i=1}^{N}\omega_z\left(\frac{x_{Ei}}{x_{EP}}-1\right)^2$$
$$\text{s.t. } E > 1, r_{Ei} \geq 0 \quad (30)$$

where the 1st term gives the estimation errors for power flow equations for all the time instants. The error at time instant k is defined as (31)

$$e_i^{ex}(k) = E - \left|\left(P_i(k) - jQ_i(k)\right)\left(r_{Ei} + jx_{Ei}\right) + \left(V_i(k)\right)^2\right| / V_i(k) \quad (31)$$

The 2nd and 3rd terms summate normalized differences in resistance r_{Ei} and reactance x_{Ei} of z_{Ei} between the estimates for the current and previous time windows. ω_e and ω_z are the weighting factors respectively for variances of E and z_{Ei} over the time window.

B. Voltage Stability Assessment Algorithm

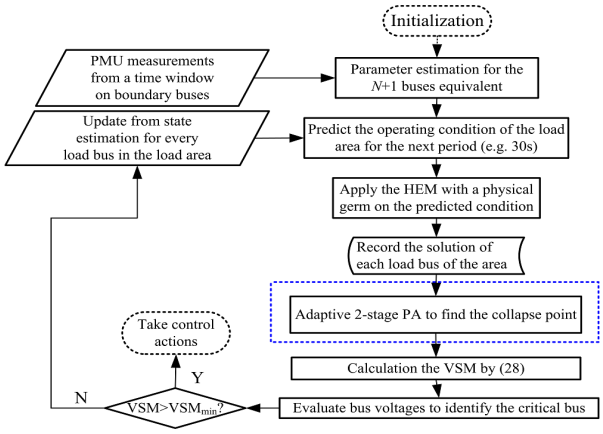

Fig. 6. Flowchart of the HEM-based online VSA scheme.

This article has been accepted for publication in a future issue of this journal, but has not been fully edited. Content may change prior to final publication. Citation information: DOI 10.1109/TPWRS.2017.2771384, IEEE Transactions on Power Systems

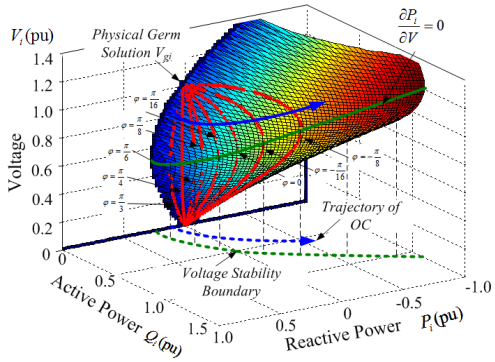

Fig. 7. Illustration of the voltage w.r.t. its active and reactive powers and the voltage stability boundary for a load bus.

As shown by the flowchart of the HEM-based online VSA scheme in Fig. 6, the scheme is applied to an offline selected load area with N branches supported by the external grid. Then, fed by the synchronized PMU measurements for a sliding time window, the parameters of the equivalent circuit can be estimated online to represent the external grid. Meanwhile, the state of each bus in the load area is updated from the state estimation. It can be assumed that the active power, reactive power and voltage of every bus of the load area are obtained from the state estimator, e.g. every 30 seconds [42]. Practically, the loads may vary randomly in a load area, so load trending prediction for the next 30 seconds is adopted. Applying the forecasted loading condition and identified parameters of the equivalent external system, the proposed HEM generates the power series for every bus regarding the overall loading scale of the load area. Further, an adaptive 2-stage PA method is used to find the accurate collapse point and then the corresponding VSM can be calculated. Additionally, the voltage of each bus with respect to overall load increase can be evaluated by plugging in the loading scale into the analytical expression of the PA. Hence, the critical bus with the lowest voltage can be identified. Finally, if the voltage margin VSM for the next period violates a pre-specified threshold VSM_{min}, control actions may be taken immediately on that critical bus.

In Fig. 7, the surface in the 3-dimensional space illustrates how the voltage magnitude of a load bus i changes with its active and reactive powers. The physical germ solution V_{gi} clearly shows the no-load condition of the load bus. The green line highlights the voltage stability boundary of the load bus i with respect to different power factors, while the arrowed blue line illustrates the trajectory of the operating condition (OC).

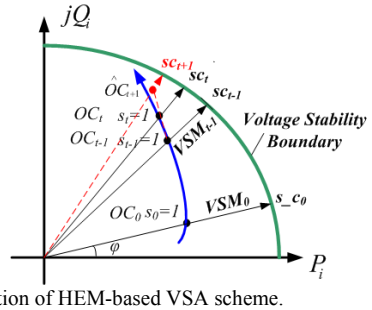

Fig. 8. Illustration of HEM-based VSA scheme.

Fig. 8 depicts the projection of Fig. 7 onto the P-Q plane to illustrate the procedure of this HEM-based online VSA scheme. The x-axis and y-axis represent the active and reactive powers of bus i. The voltage stability boundary represents the voltage collapse point with respect to different power factor angles φ. The point OC_0 is the original operating condition with $s_0 = 1$. After implementation of this proposed HEM, the P-V curve can be obtained by plugging various values of s into the power series of $V(s)$ under the assumption that all loads are scaled up simultaneously at the same rate and the power factor of each load is maintained invariant.

Then adaptive PA help to accurately predict the voltage collapse point sc_t, which will be introduced in the next sub-section. The VSM of the overall system is defined in (32), where sc_t represents the maximum loading scale at time t until the voltage collapses. VSM physically means the maximum limit of the loading scale in percentage to maintain the voltage stability of the load area.

As shown in Fig. 8, assuming the current operating condition (at time t) is the point OC_t, the load trending prediction for the next 30 seconds period is adopted, which is based on the linear extrapolation of previous periods. In (33), $S_{i,t}$ denotes the complex power of bus i at time t.

$$VSM_t = (sc_t - 1) \times 100\% \tag{32}$$

$$S_{i,t+1} = S_{i,t} + \Delta S_{i,t} = 2S_{i,t} - S_{i,t-1} \tag{33}$$

C. Considering Different Load Models

Even for steady-state analysis, load models are important in the VSA especially when voltage dependent loads exist. For example, the actual voltage collapse point no longer coincides with the nose point of the P-V curve when load cannot be modelled as 100% constant power load. A new power series about the voltage magnitude, i.e. $M_i(s) = |V_i(s)|$, should be integrated to represent the dependence between the loading level and the voltage magnitude. When ZIP load exists, the actual load varies nonlinearly with s. APPENDIX-B demonstrates the embedding method and the final matrix equation on a 3-bus system with ZIP load.

D. Computational Burden of the Proposed Scheme

After the data collected from the state estimation, the ideal computation time of the proposed VSA scheme includes three parts, i.e. (i) the time T_{Germ} for finding the physical germ solution, (ii) the time T_{PS} for finding the power series by the HEM using the physical germ solution, and (iii) the time T_{Pade} for calculating the collapse point by the adaptive PA.

$$T_{HEM} = T_{Germ} + T_{PS} + T_{Pade} \tag{34}$$

$$T_{Germ} = N_{Germ} \cdot t_M \tag{35}$$

$$T_{PS} = N_{PS} \cdot t_M \tag{36}$$

Since each term is calculated by a matrix multiplication and several convolutions, the computation times T_{Germ} and T_{PS} mainly depend on the numbers of terms required to meet the error tolerance, i.e. N_{Germ} and N_{PS} in (35) and (36), respectively. t_M indicates the average computation time for each term. Less error tolerance implies more terms in the power series to approximate the P-V curve. Practically, the maximum number of terms is in the range of 40-60 since the float point precision

This article has been accepted for publication in a future issue of this journal, but has not been fully edited. Content may change prior to final publication. Citation information: DOI 10.1109/TPWRS.2017.2771384, IEEE Transactions on Power Systems

can be exhausted [17]. The computation burden of T_{Pade} mainly depends on the number of PQ buses in the network.

Compared with the CPF, which starts from a certain power flow solution and linearly predicts and corrects an adjacent point on the P-V curve step by step using the Newton-Raphson (N-R) method, the proposed HEM has better time performance. Although it also starts from a certain point, the HEM predicts the P-V curve nonlinearly and directly to the branch point [30].

Assume that there are l slack buses, m PQ buses and p PV buses in the N-bus network. The dimension of the matrix equation equals $D_m=2l+2m+5p$ and a number of $C_m=m+2p$ convolutions are involved in the calculation of each term. The computational complexity of the proposed HEM is (37)

$$O\left(D_m^3\right)+N_{PS}\cdot O\left(D_m^2\right)+C_m N_{PS}\cdot O\left(N_{PS}{}^2\right) \quad (37)$$

The 1st term is the computational complexity of matrix inverse. The 2nd and 3rd parts are the complexities with matrix multiplications and convolutions, respectively. The HEM algorithm contains one matrix inverse operation, N_{PS} matrix multiplication operations and C_mN_{PS} convolutions.

The computational complexity of CPF also depends on the size of the network and the iterations of the prediction-correction scheme. Assume the CPF contains N_{step} prediction steps and each step contains N_{Iter} correction iterations on average. The computational complexity is (38).

$$N_{Step}N_{Iter}\left[3\cdot O\left(E_m^3\right)\right] \quad (38)$$

The computational complexity of finding the $E_m\times E_m$ ($E_m=2m+p$) Jacobian matrix per iteration is $O(E_m{}^3)$. Then the Jacobian matrix is inversed and multiplied with the error matrix of PFEs. All the 3 operations are with computational complexity of $O(E_m{}^3)$. The prediction-correction steps are normally much more than the terms of the HEM (i.e. $N_{Step}>N_{PS}$). So the proposed HEM has higher efficiency over the conventional CPF. The computation time of CPF and the proposed method will be compared in the following sections.

VI. Illustration on a 4-Bus Power System

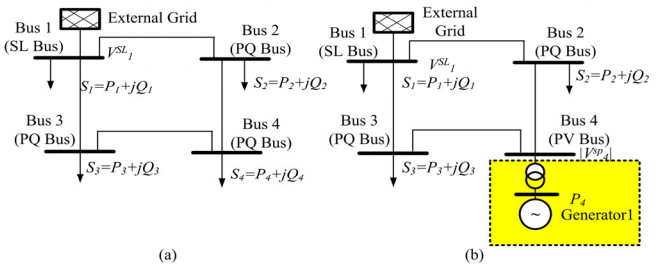

Fig. 9. 4-bus power system: (a) Case A and Case B; (b) Case C.

As shown in Fig. 9(a), a 4-bus test system modified from that in [43] is first used to demonstrate the proposed VSA approach. It has an external grid supporting three constant power loads. The external grid model is provided by the software DIgSILENT PowerFactory [44]. The time-domain simulation is executed by DIgSILENT PowerFactory with gradual load increases from the original operating condition. Then the proposed HEM-based VSA is implemented in MATLAB, and compared with the CPF using the MATPOWER 6.0 toolbox [45]. Case A and Case B are quasi-dynamic simulations considering different types of load profiles. Case C conducts dynamic simulation with ZIP models for loads and a generator connected to Bus 4 as shown in Fig. 9(b). Data for Cases A-C are given in APPENDIX-C.

A. Case A: Increasing loads at the same rate

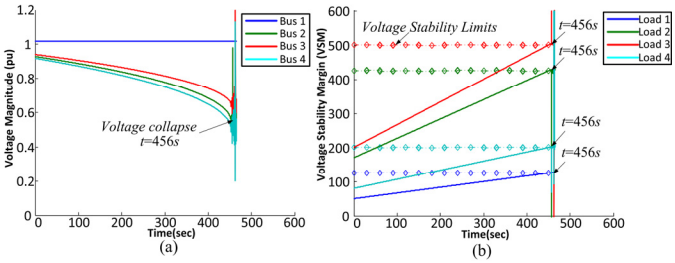

Fig. 10. Voltage magnitudes (a) and active powers vs. limits (b) for Case A.

In Case A, the power consumption of all loads is gradually ramped up at the same rate from their original loads while their power factors are kept unchanged. It can be identified by the voltage magnitudes in Fig. 10(a) that voltage collapse happens at t = 456 s, which is accurately predicted by the results from the HEM calculated every 30 seconds, as shown in Fig. 10(b), where active powers at all buses cross their respective voltage stability limits at the same time. The diamond markers connected to horizontal dash-dot lines in Fig. 10(b) indicate the voltage stability limit of each bus calculated by the HEM and updated every 30 seconds (assumed to be the time interval of state estimation). Note from Fig. 10(b) that this case has invariant voltage stability limits for all buses since all loads increase uniformly.

B. Case B: Increasing loads at different random rates with variable power factors

In the time-domain simulation of Case B, the active power and reactive power of all loads are gradually increased every 30 seconds at random rates, ranging between 0% and 30% of their original loads. Seen from voltage magnitudes of the 4-bus system in Fig. 11(a), voltage collapse happens at t = 301 s. This voltage collapse is also accurately predicted by the overall VSM calculated by (32) from the HEM in Fig. 11(b). Fig 12 compares the active and reactive powers of each load to the voltage stability limits, which are shown by the dash-dot lines and updated every 30 seconds based on the result of state estimation and load trending prediction. Also, note that, in Fig. 12(a), the active powers of loads at Buses 2, 3 and 4 cross their limits at different times, i.e. t = 290 s, 295 s and 289 s, respectively. In Fig. 12(b), the reactive power of load at Bus 4 crosses the limit at t = 290 s.

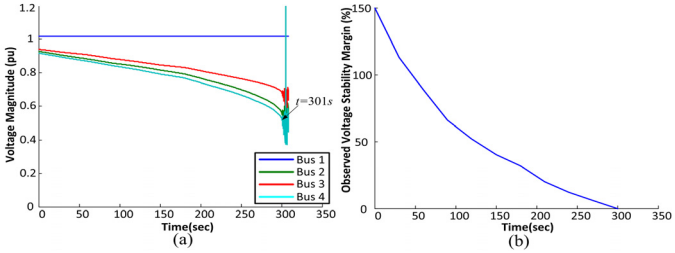

Fig. 11. Voltage magnitudes (a) and VSM (b) for Case B.

This article has been accepted for publication in a future issue of this journal, but has not been fully edited. Content may change prior to final publication. Citation information: DOI 10.1109/TPWRS.2017.2771384, IEEE Transactions on Power Systems

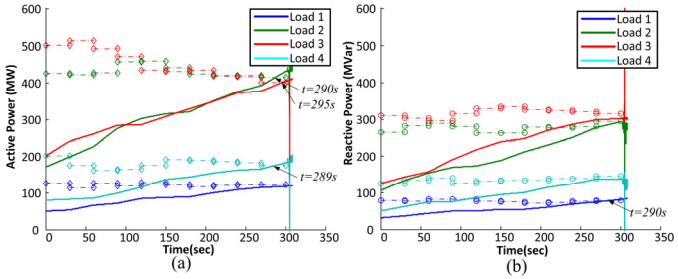

Fig. 12. Active powers (a) and reactive powers (b) vs. limits for Case B.

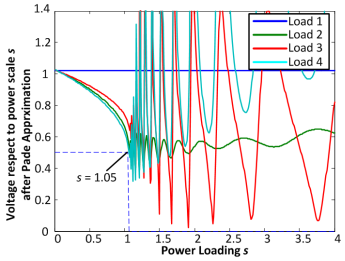

Fig. 13. Voltage vs. loading scale s at t = 240 s for Case B.

Fig. 13 shows the voltage with respect to the overall loading scale predicted by the HEM at t = 240 s. The collapse loading scale sc is 1.05, so the VSM is only 5%, which means that if the loads in the next 30 seconds ramp up at the same rate, the total load can only increase by 5% at the end of the next period, i.e. at t = 270 s. From Fig. 13, Bus 4 is the critical bus having the lowest voltage, where remedial control actions should be taken first.

C. Case C: Increasing loads at different random rates and considering ZIP load and dynamics of the generator

As shown in Fig. 9(b), Bus 4 is connected to a generator with 238MW active power output. The generator is with 6th order detailed model and equipped with IEEE Type 3 speed-governor model and IEEE Type 1 excitation model with over excitation limit. During the simulation, around 20% of the total active power load increase is picked up by the generator, while the remaining is balanced by the external grid, i.e. α_i = 20% in (25). ZIP load model is considered with the percentages of constant Z, constant I and constant P as 10%, 30% and 60% respectively.

The active and reactive powers of all loads are gradually increased at random rates, the same as Case B. Seen from voltage magnitudes of the time-domain simulation in Fig. 14(a), with voltage support from the generator at Bus 4, voltage collapse happens at t = 506 s, later than Case B. Fig. 14(b) shows the active and reactive power outputs of the generator with the over excitation limit activated at t = 357 s.

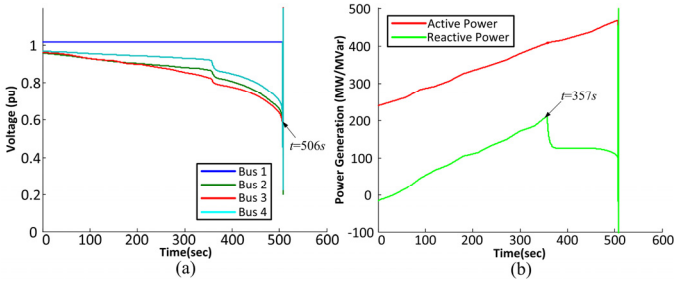

Fig. 14. Voltage magnitudes (a) and generator output (b) for Case C.

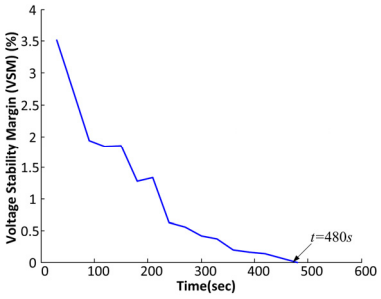

Fig. 15. VSM for Case C.

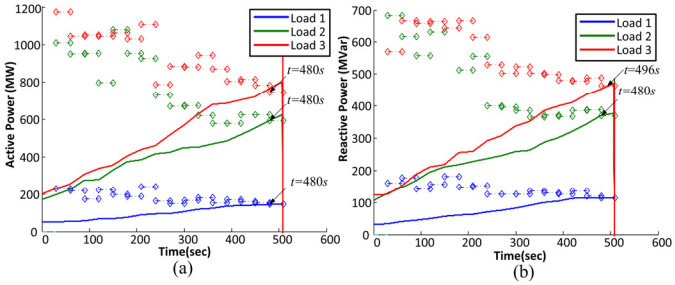

Fig. 16. Active powers (a) and reactive powers (b) vs. limits for Case C.

This voltage collapse can be predicted by the overall VSM from the HEM in Fig. 15. The VSM approaches 0 at t = 480 s. Fig. 16 compares the active and reactive powers of each load to the voltage stability limits. In Fig. 16(a), the active loads at buses 1, 2 and 3 cross their respective limits at the same time with the update of state estimation, i.e. t = 480 s. In Fig. 16(b), the reactive loads at buses 2 and 3 cross the limits at different time, i.e. t = 480 s and 496 s. Fig. 17 shows the voltage with respect to the overall loading scale screened by the HEM at t = 480 s. It can be noticed that voltage at Bus 3 has the lowest voltage and is thus identified as the critical bus where remedial actions should be taken first.

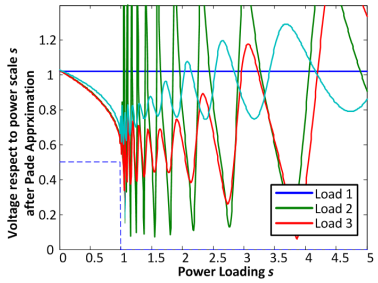

Fig. 17. Voltage vs. loading scale s at t = 480 s for Case C.

In order to show the advantage of the proposed method for VSA, the computation time is compared between the proposed HEM-based VSA and the CPF. Table II shows the maximum computation time among all scenarios using the proposed method and the CPF. The CPF is carried out in MATPOWER 6.0 adopting natural parameterization and adaptive step length control. Both algorithms are executed on a PC with Intel Core i5-3210M 2.50GHz CPU and 4GB RAM and both algorithms are configured with an error tolerance of 10e-6. It can be noted that the CPF has a number of prediction-correction steps N_{Step} and its maximum computation time among all scenarios is between 11.10 s and 20.64 s, while the proposed method is much faster, with maximum computation time between 0.873s and 1.473s. This can be simply explained by the non-iterative

This article has been accepted for publication in a future issue of this journal, but has not been fully edited. Content may change prior to final publication. Citation information: DOI 10.1109/TPWRS.2017.2771384, IEEE Transactions on Power Systems

nature of the HEM. For a single loading level with the same precision, the numbers of terms (N_{Germ} and N_{PS}) to be calculated by the proposed HEM-based VSA scheme are smaller than the steps of the CPF (N_{Step}), and each term is calculated by matrix multiplication instead of the iterative computations of the N-R method for each step of the CPF.

TABLE II.
TIME PERFORMANCES OF THE PROPOSED METHOD AND CPF METHOD

Method	HEM-based VSA						CPF	
Max.term /Time (s)	N_{Germ}	N_{PS}	T_{Germ}	T_{PS}	T_{Pade}	T_{HEM}	N_{Step}	T_{CPF}
Case A	6	14	0.003s	0.55s	0.32s	**0.873s**	232	**11.10s**
Case B	6	15	0.003s	0.64s	0.65s	**1.293s**	238	**13.33s**
Case C	6	29	0.003s	0.9s	0.57s	**1.473s**	266	**20.64s**

VII. CASE STUDY ON THE NPCC POWER SYSTEM

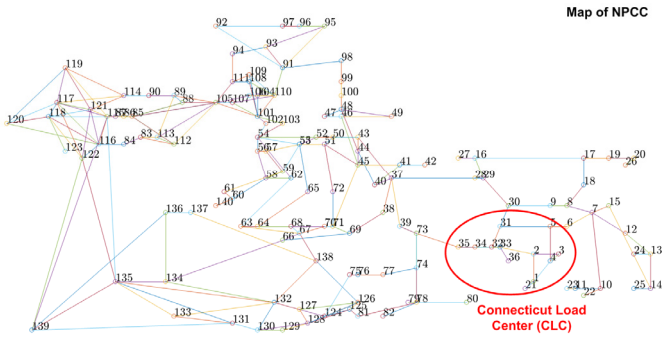

Fig. 18. Map of NPCC system and the CLC load area.

The NPCC system with 48 generators and 140 buses in [46] is adopted to demonstrate the proposed HEM-based VSA method. As shown in Fig. 18, the Connecticut Load Center (CLC) area is supported by three tie lines, i.e. 73-35, 30-31 and 6-5. Assume that all 3 tie lines are equipped with PMUs at boundary buses 35, 31 and 5 of the load area. PowerFactory is used to simulate the voltage instability scenarios in the following cases. The load at each bus of the area is modelled as constant power load. All buses in load area are measured by SCADA system and the state estimation results on the load area are also assumed to be updated every 30 seconds. Thus, the HEM-based VSA scheme aims at predicting voltage instability in the next 30 seconds period.

A. Case D: Increasing loads at same rate

II. In the dynamic simulation of Case D, loads at all buses of the area increase at a same rate of 0.16% per second. Fig. 19(a) shows that voltages gradually decrease and then collapse at t = 456.3 s. The external system is aggregated to an equivalent voltage source E directly connected to three boundary buses of the load area by three branches. Fig. 19(b) gives the estimates of the branch impedance to buses 31, 35 and 5. Voltage collapse is predicted when the active and reactive powers meeting their limits during t = 420-450 s, as shown by dash-dot lines in Fig. 20. Compared to Case A of the 4-bus system, the variations in stability limits are caused by the changes in the external system and consequently in their equivalent parameters. As shown in Fig. 21(a), at t = 420 s the VSM decreases to only 3%. Assuming a threshold of control activation is preset, e.g. 10%, the action should have been taken, e.g. switching in a shunt capacitor at the critical bus having the lowest voltage, i.e. Bus 34. Fig. 21(b) gives the voltage with respect to loading scale s predicted by the HEM at t = 420 s, and a precise collapse load scale sc = 1.03.

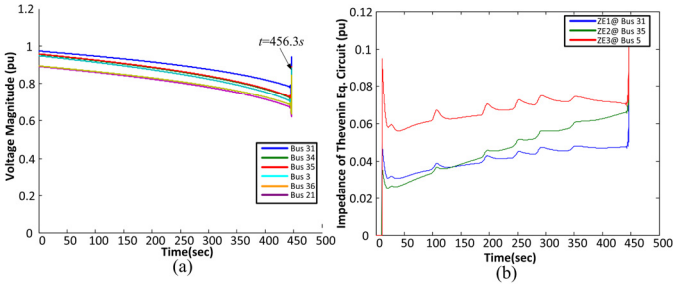

Fig. 19. Voltage magnitudes (a) and online estimated impedances' magnitude (b) of equivalent branches for Case D.

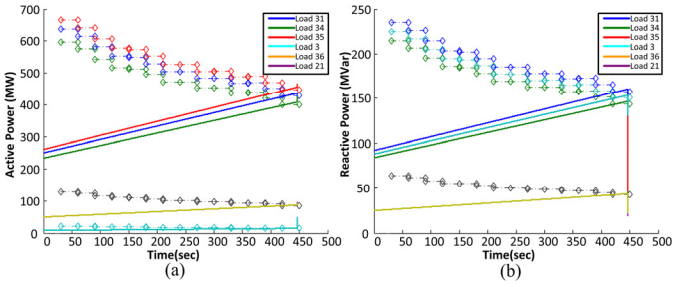

Fig. 20. Active powers (a) and reactive powers (b) vs. limits for Case D.

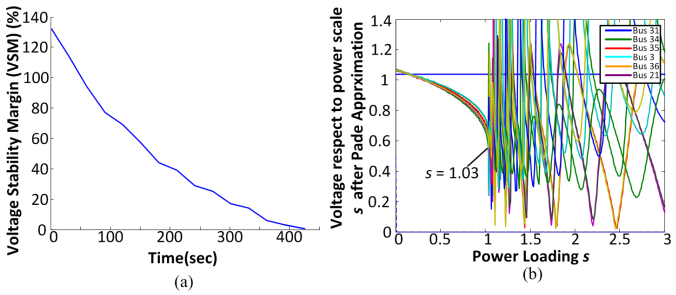

Fig. 21. (a)VSM and (b) Voltage vs. loading scale at t = 420 s for Case D.

A. Case E: Increasing loads at different random rates with variable power factors

In this case, a more realistic scenario with loads increasing at a random rate in 0-10% every 30 seconds is tested. Voltage collapse happens at t = 452 s, as shown in Fig. 22. The last warning should be armed between t = 420 s and t =450 s with a more conservative threshold, since loads at Buses 31, 34, 35 and 3 cross their individual stability limits at t = 450 s, as shown in Fig. 23 (a) and (b) for active and reactive powers, respectively. From Fig. 24, the VSM drops to 0 at t = 450 s, indicating the occurrence of voltage instability.

The online HEM-based VSA scheme is able to provide system operators with a timely and accurate indication of the VSM. Practically, a more conservative threshold of VSMs should be preset, e.g. 5-10%. On one hand, that gives operators enough time to activate emergency voltage control; on the other hand, it leaves enough stability margin to prevent voltage collapse. All computations of this new scheme can be finished within 2 seconds in MATLAB, including external

This article has been accepted for publication in a future issue of this journal, but has not been fully edited. Content may change prior to final publication. Citation information: DOI 10.1109/TPWRS.2017.2771384, IEEE Transactions on Power Systems

parameter identification, load flow trending prediction, the proposed HEM, and adaptive PA, so the overall VSM and individual VSM for each bus is predicted about 28 seconds ahead. If each bus is equipped with a PMU to provide synchronized phasor data at a higher frequency, e.g. 30-60Hz, operators can monitor the load change and the VSM at each load bus with higher accuracy so as to decide more precisely whether and when a remedial action is needed.

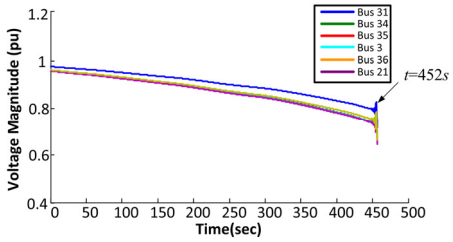

Fig. 22. Voltage magnitudes for Case E.

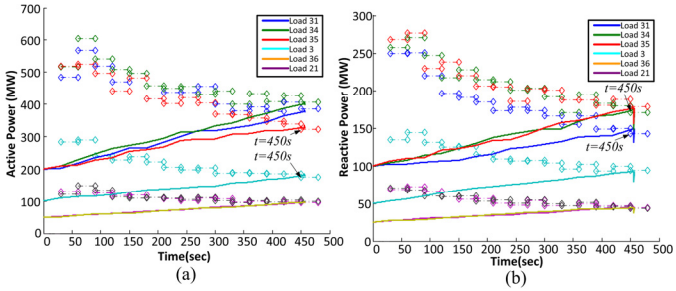

Fig. 23. Active powers (a) and reactive powers (b) vs. limits for Case E.

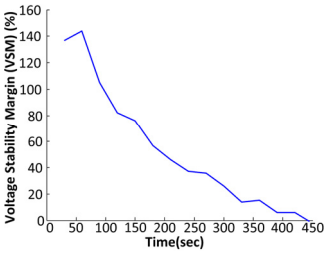

Fig. 24. VSM for Case E.

Table III compares the maximum computation time among all scenarios in Case D and Case E using the proposed method and the CPF with the same error tolerance, i.e. 10e-6. It can be noted that the proposed HEM-based VSA scheme has better time performance.

TABLE III.
COMPARISON OF MAXIMUM COMPUTATION TIME BETWEEN THE PROPOSED METHOD AND THE CONTINUATION POWER FLOW METHOD

Method	**HEM-based VSA**						**CPF**	
Max.term /Time (s)	N_{Germ}	N_{PS}	T_{Germ}	T_{PS}	T_{Pade}	T_{HEM}	N_{Step}	T_{CPF}
Case D	8	21	0.005s	0.9s	0.52s	**1.425s**	228	**14.10s**
Case E	8	23	0.005s	1.1s	0.63s	**1.735s**	235	**16.36s**

VIII. CONCLUSION

This paper proposes a new online VSA scheme for a load area based on a new HEM with a physical germ solution. The physical germ solution endows the physical meaning of the analytical expression, i.e. the loading level. Based on the HEM result, the scheme can online monitor the VSM of a load area, predict the voltage instability and suggest system operators the timing and location to take remedial actions. An adaptive two-stage PA method is also proposed to extend the convergence region of the power series, making the prediction of voltage collapse more accurate. These methods jointly enable the performance of this new VSA scheme and are demonstrated on a 4-bus system and the 140-bus NPCC system. Compared with model-based VSA methods, the proposed scheme has better online time performance by using the non-iterative HEM to give the whole P-V curve. Unlike most of measurement-based methods, it avoids network reduction in the load area. Also, this scheme can integrate load trending prediction at each bus for look-ahead stability monitoring.

APPENDIX A PHYSICAL GERM SOLUTION OF A 3-BUS SYSTEM

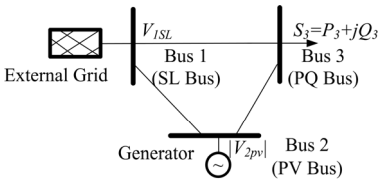

Fig. 25. The demonstrative 3-bus system.

A 3-bus system having 1 slack bus, 1 PV bus and 1 PQ bus, shown in Fig. 25, is adopted to illustrate the procedure of finding a physical germ solution. The first step is to calculate the starting no-load no-generation condition. Only the slack bus propagates its voltage to the whole passive network:

$$\begin{bmatrix} 1 & & & & & & \\ & 1 & & & & & \\ G_{21} & -B_{21} & G_{22} & -B_{22} & G_{23} & -B_{23} \\ B_{21} & G_{21} & B_{22} & G_{22} & B_{23} & G_{23} \\ G_{31} & -B_{31} & G_{32} & -B_{32} & G_{33} & -B_{33} \\ B_{31} & G_{31} & B_{32} & G_{32} & B_{33} & -B_{33} \end{bmatrix} \begin{bmatrix} V_{ST1re} \\ V_{ST1im} \\ V_{ST2re} \\ V_{ST2im} \\ V_{ST3re} \\ V_{ST3im} \end{bmatrix} = \begin{bmatrix} \mathrm{Re}\left(V_1^{SL}\right) \\ \mathrm{Im}\left(V_1^{SL}\right) \\ 0 \\ 0 \\ 0 \\ 0 \end{bmatrix} \quad \text{(A1)}$$

The second step is to find the physical germ solution by an embedding. The right hand side of the PQ bus (i.e. Bus 3) is 0, since no-load condition is held for the physical germ solution. Thus, the embedding of PV bus (i.e. Bus 2) is needed to adjust its voltage magnitude to the specified value $|V_{2pv}|$, while keep the active power generation as the specified value P_2.

Move all the n^{th} order terms (i.e. the unknowns) to the left hand side and leave terms 0 to (n-1) (i.e. the knowns) on the right hand side of (A2). The matrix equation is extended by moving the unknown variables of PV bus (Bus 2), i.e. $W_{g2re}[n]$, $W_{g2im}[n]$ and $Q_{g2}[n]$ to the left hand side.

$$\begin{bmatrix} 1 & 0 & 0 & 0 & 0 & 0 & 0 & 0 & 0 \\ 0 & 1 & 0 & 0 & 0 & 0 & 0 & 0 & 0 \\ G_{21} & -B_{21} & G_{22} & -B_{22} & G_{23} & -B_{23} & 0 & 0 & W_{ST2im} \\ B_{21} & G_{21} & B_{22} & G_{22} & B_{23} & G_{23} & 0 & 0 & W_{ST2re} \\ G_{31} & -B_{31} & G_{32} & -B_{32} & G_{33} & -B_{33} & 0 & 0 & 0 \\ B_{31} & G_{31} & B_{32} & G_{32} & B_{33} & -G_{33} & 0 & 0 & 0 \\ 0 & 0 & W_{ST2re} & -W_{ST2im} & 0 & 0 & V_{ST2re} & -V_{ST2im} & 0 \\ 0 & 0 & W_{ST2im} & W_{ST2re} & 0 & 0 & V_{ST2im} & V_{ST2re} & 0 \\ 0 & 0 & V_{ST2re} & V_{ST2im} & 0 & 0 & 0 & 0 & 0 \end{bmatrix} \begin{bmatrix} V_{g1re}[n] \\ V_{g1im}[n] \\ V_{g2re}[n] \\ V_{g2im}[n] \\ V_{g3re}[n] \\ V_{g3im}[n] \\ W_{g2re}[n] \\ W_{g2im}[n] \\ Q_{g2}[n] \end{bmatrix} = \begin{bmatrix} 0 \\ 0 \\ \mathrm{Re}\left(P_2 W_{g2}[n-1] + \underset{1}{\overset{n-1}{Conv}}(Q_{g2} * W_{g2}^*)\right) \\ \mathrm{Im}\left(P_2 W_{g2}[n-1] + \underset{1}{\overset{n-1}{Conv}}(Q_{g2} * W_{g2}^*)\right) \\ 0 \\ 0 \\ -\mathrm{Re}\left(\underset{1}{\overset{n-1}{Conv}}(W_{g2} * V_{g2})\right) \\ -\mathrm{Im}\left(\underset{1}{\overset{n-1}{Conv}}(W_{g2} * V_{g2})\right) \\ \varepsilon_2[n-1] \end{bmatrix} \quad \text{(A2)}$$

where

$$\underset{1}{\overset{n-1}{Conv}}(Q_{g2} * W_{g2}^*) = \sum_{m=1}^{n-1} Q_{g2}[n-m] W_{g2}^*[m] \quad \text{(A3)}$$

This article has been accepted for publication in a future issue of this journal, but has not been fully edited. Content may change prior to final publication. Citation information: DOI 10.1109/TPWRS.2017.2771384, IEEE Transactions on Power Systems

$$\underset{1}{\overset{n-1}{Conv}}(W_{g2} * V_{g2}) = \sum_{m=1}^{n-1} W_{g2}[n-m]V_{g2}[m] \tag{A4}$$

APPENDIX B CONSIDERING ZIP LOAD FOR PQ BUSES

Consider a PQ bus i with ZIP load given by (A5), where p_Z, p_I and p_P are the percentages of constant impedance, current and power components in active power load P_i, and q_Z, q_I and q_P are the percentages of constant impedance, current and power components of reactive power load Q_i. P_{i0} and Q_{i0} are the active and reactive powers at the voltage equal to 1.0pu. The PFE for each ZIP load bus becomes (A6) and (A7).

$$\begin{cases} P_i = P_{i0}(p_Z |V_i|^2 + p_I |V_i| + p_P) \\ Q_i = Q_{i0}(q_Z |V_i|^2 + q_I |V_i| + q_P) \end{cases}, \quad \forall i \in \boldsymbol{\mathcal{P}} \tag{A5}$$

$$\sum_{k=1}^{N} Y_{ik} V_k(s) = \frac{s\left(P_{i0}(p_Z |V_i|^2 + p_I |V_i| + p_P) - jQ_{i0}(q_Z |V_i|^2 + q_I |V_i| + q_P)\right)}{V_i^*(s^*)} \tag{A6}$$

$$\sum_{k=1}^{N} Y_{ik}\left(V_k[0] + V_k[1]s + V_k[2]s^2 + \cdots\right) = s\left\{S_{Zi}^* V_i(s) + \frac{S_{Pi}^* + S_{Ii}^* |V_i|(s)}{V_i^*(s^*)}\right\}$$
$$= sS_{Zi}^*\left(V_i[0] + V_i[1]s + \cdots\right) + sS_{Pi}^*\left(W_{ig}^* + W_i^*[1]s + \cdots\right) + sS_{Ii}^*\left(M_i[0] + M_i[1]s + \cdots\right)\left(W_{ig}^* + W_i^*[1]s + \cdots\right) \tag{A7}$$

where S_{Zi}, S_{Ii}, S_{Pi} are the complex power of the load for constant impedance, current and power components respectively at bus i and $M_i(s)$ is the series of voltage magnitude at bus i, i.e. $M_i(s) = |V_i(s)|$, satisfying (A9)

$$\begin{cases} S_{Zi} = P_{i0} p_Z + jQ_{i0} q_Z \\ S_{Ii} = P_{i0} p_I + jQ_{i0} q_I \\ S_{Pi} = P_{i0} p_P + jQ_{i0} q_P \end{cases} \tag{A8}$$

$$M_i(s) \cdot M_i(s) = V_i(s) \cdot V_i^*(s^*) \tag{A9}$$

Finally, if the ZIP load model is considered, the final recursive matrix equation of the demonstrative 3-bus system in Appendix A becomes (A10) and (A11).

$$\begin{bmatrix} 1 & 0 & 0 & 0 & 0 & 0 & 0 & 0 & 0 \\ 0 & 1 & 0 & 0 & 0 & 0 & 0 & 0 & 0 \\ G_{21} & -B_{21} & G_{22} & -B_{22} & G_{23} & -B_{23} & -P_{g2} & Q_{g2} & W_{g2im} \\ B_{21} & G_{21} & B_{22} & G_{22} & B_{23} & G_{23} & Q_{g2} & P_{g2} & W_{g2re} \\ G_{31} & -B_{31} & G_{32} & -B_{32} & G_{33} & -B_{33} & 0 & 0 & 0 \\ B_{31} & G_{31} & B_{32} & G_{32} & B_{33} & -G_{33} & 0 & 0 & 0 \\ 0 & 0 & W_{g2re} & -W_{g2im} & 0 & 0 & V_{g2re} & -V_{g2im} & 0 \\ 0 & 0 & W_{g2im} & W_{g2re} & 0 & 0 & V_{g2im} & V_{g2re} & 0 \\ 0 & 0 & V_{g2re} & V_{g2im} & 0 & 0 & 0 & 0 & 0 \end{bmatrix} \begin{bmatrix} V_{1re}[n] \\ V_{1im}[n] \\ V_{2re}[n] \\ V_{2im}[n] \\ V_{3re}[n] \\ V_{3im}[n] \\ W_{2re}[n] \\ W_{2im}[n] \\ Q_2[n] \end{bmatrix}$$

$$= \begin{bmatrix} 0 \\ 0 \\ \mathrm{Re}\left(\underset{1}{\overset{n-1}{Conv}}(Q_2 * W_2^*)\right) \\ \mathrm{Im}\left(\underset{1}{\overset{n-1}{Conv}}(Q_2 * W_2^*)\right) \\ \mathrm{Re}\left(S_{3P}^* W_3^*[n-1] + S_{3Z}^* V_3[n-1] + S_{3I}^* \underset{0}{\overset{n-1}{Conv}}(M_3 * W_3^*)\right) \\ \mathrm{Im}\left(S_{3P}^* W_3^*[n-1] + S_{3Z}^* V_3[n-1] + S_{3I}^* \underset{0}{\overset{n-1}{Conv}}(M_3 * W_3^*)\right) \\ -\mathrm{Re}\left(\underset{1}{\overset{n-1}{Conv}}(W_2 * V_2)\right) \\ -\mathrm{Im}\left(\underset{1}{\overset{n-1}{Conv}}(W_2 * V_2)\right) \\ \delta_{n1} \cdot \frac{1}{2}\left(|V_2^{sp}|^2 - |V_{g2}|^2\right) - \frac{1}{2}\left(\sum_{m=1}^{n-1} V_2[m] V_2^*[n-m]\right) \end{bmatrix} \tag{A10}$$

where

$$\underset{0}{\overset{n-1}{Conv}}(M_3 * W_3^*) = \sum_{m=0}^{n-1} M_3[n-m] W_3^*[m] \tag{A11}$$

APPENDIX C DATA OF THE 4-BUS SYSTEM

Data of the 4-bus system in Section V are given in Tables IV-VI respectively for transmission lines, buses (Cases A-C), and the generator.

TABLE IV. TRANSMISSION LINE DATA FOR 4-BUS SYSTEM

From Bus -To Bus	Resistance R (pu)	Reactance X (pu)	Shunt admittance Y (pu)
1-2	0.01008	0.0504	0.1025
1-3	0.00744	0.0372	0.0775
2-4	0.00744	0.0372	0.0775
3-4	0.01272	0.0636	0.1275

TABLE V. BUS DATA FOR 4-BUS SYSTEM FOR CASES A-C

Bus No.	Bus Type	V_{sp}(pu)	Generation		Load	
			P_G(MW)	Q_G(MVar)	P_L(MW)	Q_L(MVar)
1	SL	1.02	-	-	50	30.99
2	PQ	-	0	0	170	105.35
3	PQ	-	0	0	200	123.94
4	PQ	-/0.98	0/238	0/ [-100, 200]	80	49.58

TABLE VII. GENERATOR DATA FOR CASE C

$\boldsymbol{H}$	Inertia time constant (s)	4.2
$\boldsymbol{x_l}$	Leakage reactance (p.u.)	0.125
$\boldsymbol{X_d, X_q}$	Synchronous reactances (p.u.)	1, 0.69
$\boldsymbol{X_d', X_q'}$	Transient reactances (p.u.)	0.31, 0.5
$\boldsymbol{X_d'', X_q''}$	Sub-transient reactances (p.u.)	0.25, 0.25
$\boldsymbol{T_{d0}', T_{q0}'}$	Transient time constants (s)	10.2, 0.41
$\boldsymbol{T_{d0}'', T_{q0}''}$	Sub-transient time constants (s)	0.05, 0.035

REFERENCES

[1] B. Gao *et al.*, "Voltage stability evaluation using modal analysis," *IEEE Trans. Power Syst.*, vol. 7, no. 4, pp. 1529-1542, Nov. 1992.

[2] Y. Mansour *et al.*, "SVC placement using critical modes of voltage instability," *IEEE Trans. Power Syst.*, vol. 9, no. 2, pp. 757-763, May 1994.

[3] T. Van Cutsem, C. Vournas, *Voltage Stability of Electric Power Systems*, Norwell, MA: Kluwer, 1998.

[4] P. Löf *et al.*, "Fast calculation of a voltage stability index," *IEEE Trans. Power Syst.*, vol. 7, no. 1, pp. 54-64, Feb. 1992.

[5] J. M. Lim *et al.*, "SVD-based voltage stability assessment from phasor measurement unit data," *IEEE Trans. Power Syst.*, vol. 31, no. 4, pp. 2557-2565, Jul. 2016.

[6] S. Greene *et al.*, "Sensitivity of the loading margin to voltage collapse with respect to arbitrary parameters," *IEEE Trans. Power Syst.*, vol. 12, no. 1, pp. 262-272, Feb. 1997.

[7] F. Capitanescu *et al.*, "Unified sensitivity analysis of unstable or low voltages caused by load increases or contingencies," *IEEE Trans. Power Syst.*, vol. 20, no. 1, pp. 321-329, Feb. 2005.

[8] T. Gou *et al.*, "Identification of generic bifurcation and stability problems in power system differential-algebraic model," *IEEE Trans. Power Syst.*, vol. 9, pp. 1032-1044, May 1994.

[9] W. Marszalek *et al.*, "Singularity-induced bifurcations in electrical power systems," *IEEE Trans. Power Syst.*, vol. 20, pp. 312-320, Feb. 2005.

[10] V. Ajjarapu *et al.*, "The continuation power flow: a tool for steady state voltage stability analysis," *IEEE Trans. Power Syst.*, vol. 7, no. 1, pp. 416–423, Feb. 1992.

[11] K. Vu *et al.*, "Use of local measurements to estimate voltage-stability margin," *IEEE Trans. Power Syst.*, vol. 14, no. 3, pp. 1029-1035, Aug. 1999.

[12] B. Milosevic, M. Begovic, "Voltage-stability protection and control using a wide-area network of phasor measurements," *IEEE Trans. Power Syst.*, vol. 18, no. 1, pp. 121–127, Feb. 2003.

[13] M. Glavic and T. Van Cutsem, "Wide-area detection of voltage instability from synchronized phasor measurements. Part I: Principle," *IEEE Trans. Power Syst.*, vol. 24, no. 3, pp. 1408–1416, Aug. 2009.

[14] K. Sun, P. Zhang, L. Min, "Measurement-based voltage stability monitoring and control for load centers," EPRI Technical Report No. 1017798, 2009.
[15] F. Hu, K. Sun, *et al*, "Measurement-based voltage stability assessment for load areas addressing n-1 cContingencies," *IET Generation, Transmission & Distribution,* in press
[16] F. Hu, K. Sun *et al*. "Measurement-based real-time voltage stability monitoring for load areas", *IEEE Trans. Power Systems*, vol. 31, no. 4, pp. 2787-2798, Jul. 2016.
[17] K. Sun, F. Hu, N. Bhatt, "A New Approach for Real-Time Voltage Stability Monitoring Using PMUs," IEEE PES ISGT Asia Conference, May 20-23, 2014, Kuala Lumpur, Malaysia
[18] A. Trias, "The Holomorphic Embedding Load Flow Method," *IEEE PES GM,* San Diego, CA, Jul. 2012.
[19] A. Trias, "System and method for monitoring and managing electrical power transmission and distribution networks," US Patents 7 519 506 and 7 979 239, 2009–2011.
[20] A. Trias, "Fundamentals of the holomorphic embedding load–flow method" *arXiv: 1509.02421v1*, Sep. 2015.
[21] S. S. Baghsorkhi and S. P. Suetin, "Embedding AC Power Flow with Voltage Control in the Complex Plane: The Case of Analytic Continuation via Padé Approximants," *arXiv:1504.03249*, Mar. 2015.
[22] M. K. Subramanian, *et al*, "PV bus modeling in a holomorphically embedded power-flow formulation," *North American Power Symposium (NAPS)*, Manhattan, KS, 2013.
[23] M. K. Subramanian, "Application of Holomorphic Embedding to the Power-Flow Problem," *Master Thesis*, Arizona State Univ., Aug. 2014.
[24] A. Trias, "Fundamentals of the Holomorphic Embedding Load-Flow Method," *arXiv.org*: 1509.02421, Sep. 2015.
[25] I. Wallace *et al.*, "Alternative PV bus modelling with the holomorphic embedding load flow method," *arXiv:1607.00163*, Jul. 2016
[26] S. S. Baghsorkhi *et al.*, "Embedding AC power flow in the complex plane part I: modelling and mathematical foundation," *arXiv:1604.03425*, Jul. 2016
[27] S. Rao, *et al*, "The holomorphic embedding method applied to the power-flow problem," *IEEE Trans. Power Syst.*, vol. 31, no. 5, pp. 3816-3828, Sep. 2016.
[28] C. Liu, *et al*, "A multi-dimensional holomorphic embedding method to solve AC power flows," *IEEE Access*, in press (10.1109/ACCESS.2017.2768958).
[29] S. Rao *et al.*, "Estimating the saddle-node bifurcation point of static power systems using the holomorphic embedding method," *International Journal of Electrical Power and Energy Systems*, vol. 84, no. x, pp. 1-12, 2017.
[30] B. Wang, C. Liu, K. Sun, "Multi-stage holomorphic embedding method for calculating the power-voltage curve," *IEEE Trans. Power Syst.*, in press (DOI: 10.1109/TPWRS.2017.2711260).
[31] A. Trias, J. L. Marin, "The holomorphic embedding loadflow method for DC power systems and nonlinear DC circuits," *IEEE Trans. Circuits and Systems-I: regular papers*, vol. 63, no.2, pp. 322-333, Sep. 2016.
[32] Y. Feng and D. Tylavsky, "A novel method to converge to the unstable equilibrium point for a two-bus system," *North American Power Symposium (NAPS)*, Manhattan, KS, 2013.
[33] Y. Feng, "Solving for the low-voltage-angle power-flow solutions by using the holomorphic embedding method," *Ph.D. Dissertation*, Arizona State Univ., Jul. 2015.
[34] S. Rao, D. Tylavsky, "Nonlinear network reduction for distribution networks using the holomorphic embedding method," *North American Power Symposium (NAPS)*, Denver, CO, USA, 2016.
[35] S. S. Baghsorkhi, S. P. Suetin, "Embedding AC power flow in the complex plane part II: a reliable framework for voltage collapse analysis," *arXiv:1609.01211*, Sep. 2016
[36] B Schmidt, "Implementation and evaluation of the holomorphic embedding load flow method," *Master Thesis*, Technical Univ. Munchen, Mar. 2015.
[37] M. R. Range, *Holomorphic Functions and Integral Representations in Several Complex Variables*, Springer-Verlag, New York, Inc. 2002.
[38] H. Stahl, "On the convergence of generalized Pade approximants," *Constructive Approximation*, vol. 5, pp. 221-240, 1989.
[39] H. Stahl, "The convergence of Pade approximants to functions with branch points," *J. of Approx. Theory*, vol. 91, no. 2, pp. 139-204, 1997.
[40] A. Cuyt *et al. Handbook of Continued Fractions for Special Functions*, Springer, ISBN: 978-1-4020-6948-2.
[41] J. Nocedal, S. J. Wright, *Numerical Optimization*, 2nd ed. New York, NY, USA: Springer, 2006.
[42] A. Abur, A. G. Exposito, *Power System State Estimation*, Marcel Dekker, New York, Inc. 2004.
[43] J. Grainger *et al*. *Power System Analysis*, McGraw-Hill, 1994.
[44] PowerFactory, *Technical Reference Documentation—External Grid*.
[45] R. D. Zimmerman *et al.*, "MATPOWER: Steady-state operations, planning, and analysis tools for power systems research and education," *IEEE Trans. Power Syst.*, vol. 26, no. 1, pp. 12–19, Feb. 2011.
[46] J. H. Chow *et al.*, "Inertial and slow coherency aggregation algorithms for power system dynamic model reduction," *IEEE Trans. Power Syst.*, vol. 10, no. 2, pp. 680-685, May 1995.

Chengxi Liu received his B. Eng. and M. Sc. degrees in Huazhong University of Science and Technology, China, in 2005 and 2007 respectively. He received the Ph.D. degree at the Department of Energy Technology, Aalborg University, Denmark in 2013. He worked in Energinet.dk, the Danish TSO, until 2016. Currently He is a Research Associate at the Department of EECS, University of Tennessee, USA. His research interests include power system stability and control, renewable energies and the applications of artificial intelligence.

Bin Wang (S'14) received the B. S. and M.S. degrees in Electrical Engineering from Xi'an Jiaotong University, China, in 2011 and 2013, respectively. He is currently pursuing the Ph.D. degree at the Department of EECS, University of Tennessee in Knoxville. His research interests include power system nonlinear dynamics, stability and control.

Fengkai Hu received the B.S. and M.S. degrees in automation from University of Electronic Science and Technology of China in 2009 and 2012, respectively. He received the Ph.D. degree in electrical engineering from the University of Tennessee, Knoxville in 2016. Currently, he is a power systems engineer at Siemens Industry, Inc. His research interests include power system stability and control, energy market, wide area measurement system and Distributed Energy Resources.

Kai Sun (M'06–SM'13) received the B.S. degree in automation in 1999 and the Ph.D. degree in control science and engineering in 2004 both from Tsinghua University, Beijing, China. He is currently an associate professor at the Department of EECS, University of Tennessee in Knoxville. He was a project manager in grid operations and planning at EPRI, Palo Alto, CA from 2007 to 2012. Dr. Sun is an editor of IEEE Transactions on Smart Grid and an associate editor of IET Generation, Transmission and Distribution. His research interests include power system dynamics, stability and control and complex systems.

Claus Leth Bak received the B.Sc. with honors in Electrical Power Engineering in 1992 and the M.Sc. in Electrical Power Engineering at the Department of Energy Technology at Aalborg University, Denmark in 1994. After his studies he worked as a professional engineer with Electric Power Transmission and Substations with specializations within the area of Power System Protection at the NV Net TSO. In 1999 he was employed as an Assistant Professor at ET-AAU, where he holds a Full Professor position today. He received the PhD degree in 2015. His main Research areas include Corona Phenomena on Overhead Lines, Power System Modeling and Transient Simulations, Underground Cable transmission, Power System Harmonics, Power System Protection and HVDC-VSC Offshore Transmission Networks.